Twist singularities for symplectic maps

H. R. Dullin[a)]
Department of Mathematical Sciences, Loughborough University, Loughborough LE11 3TU, United Kingdom

J. D. Meiss[b)]
Department of Applied Mathematics, University of Colorado, Boulder, Colorado 80309-0526

Received 24 June 2002; accepted 24 October 2002; published 7 January 2003)

Near a nonresonant, elliptic fixed point, a symplectic map can be transformed into Birkhoff normal form. In these coordinates, the dynamics is represented entirely by the Lagrangian ''frequency map'' that gives the rotation number as a function of the action. The twist matrix, given by the Jacobian of the rotation number, describes the anharmonicity in the system. When the twist is singular the frequency map need not be locally one-to-one. Here we investigate the occurrence of fold and cusp singularities in the frequency map. We show that folds necessarily occur near third order resonances. We illustrate the results by numerical computations of frequency maps for a quadratic, symplectic map. © *2003 American Institute of Physics.* [DOI: 10.1063/1.1529450]

The dynamics in the neighborhood of a linearly stable periodic orbit of a Hamiltonian flow or fixed point of a symplectic map can be elucidated by consideration of their Birkhoff normal forms. The normal form has action variables, J, which are formal invariants when the rotation vector, ω, of the elliptic orbit 408C448.6(408C448.6(t,)-37.8(fo86.9(ehe)43BT 2(nor6 -1.6.16 [(tion)-448.ionju8(the)]TJ (linglh

an elliptic fixed point. If we assume there are no low-order resonances, the map can be transformed to Birkhoff form to some finite order in a power series expansion in the actions. We compute the twist and show that it generally vanishes near several resonances. We compare the calculations of the twist with numerical calculations of the frequency map based on Laskar's algorithm[20,21] to observe the folds and cusps. Finally we use the technique of Meiss[22] to estimate the volume of the elliptic region in the neighborhood of the fixed point.

II. VANISHING TWIST

Since the frequency map is generated by S through $\Omega(J) = DS$, this map is an example of a "Lagrangian map." Recall that a d-dimensional submanifold of a symplectic manifold is Lagrangian if the symplectic form vanishes identically for any pair of tangent vectors to the submanifold. The submanifold $L = \{(\ ,J):\ = 0\}$ is Lagrangian, and its image under the Birkhoff normal form 1), $f(L) = \{(\ ,J):\ = DS(J)\}$, is therefore also Lagrangian. Since this Lagrangian manifold is a graph over J, we can trivially project out the J direction, defining

$$\overset{\Omega}{J \mapsto DS\ J)}!$$

$$\Omega_c \; 5 \; 2 \; 2 \epsilon \begin{pmatrix} 3J_2^2 \\ 4J_2^3 \end{pmatrix}.$$

$$\mu_k = e^{2\pi i \alpha_k}, \quad k = 1,\ldots,d. \tag{8}$$

Since the multipliers come in reciprocal pairs, we can always choose $\alpha_k \in (0,\frac{1}{2})$, for then the reciprocal multiplier corresponds to negative rotation number. With this convention, the traces, $\beta_k = 2\cos 2\pi\alpha_k$ and the residues,

$$R_k = \sin^2 \pi\alpha_k = \tfrac{1}{4}|\mu_k - 1|^2, \tag{9}$$

are one-to-one in α_k.

A. Kinematics of resonances

In the neighborhood of an elliptic fixed point, a map can be transformed into the Birkhoff normal form 1) to arbitrary

$$m \cdot \quad 5\, n. \qquad 11)$$

Thus, in frequency space, a resonance corresponds to a codimension-one plane, and the set of all resonances is the set of planes with integral normal vectors, m, and rational intercepts with the coordinate axes. Thus, the collection of resonances can be labeled by vectors $(m,n) \in {}^{d1}$

points, we start with that assumption to construct our example. In the Appendix we will show how to obtain our map from Moser's general quadratic map.

We will use a Lagrangian generating function to write our map in ''standard'' form,

$$L\ x,x')\ 5\ K\ x'\ 2\ x)\ 2\ V\ x), \tag{16}$$

where K is the ''kinetic'' and V is the ''potential'' energy. The map is generated via the one form $y'dx'\ 2\ ydx\ 5\ dL$, giving

$$\begin{aligned} y\ 5\ 2\ \frac{\partial L}{\partial x}\ 5\ DK\ x'\ 2\ x)\ 1\ DV\ x), \\ y'\ 5\ \frac{\partial L}{\partial x'}\ 5\ DK\ x'\ 2\ x). \end{aligned} \tag{17}$$

If this map has a fixed point, then we can shift it to the origin. The new generating function then has no linear terms in V.

First we consider the quadratic Lagrangian when there is a strongly-stable fixed point at the origin. In this case coordinates in phase space can be chosen so that the map is in real block diagonal normal form see, e.g., Ref. 2). Such a map is generated by a quadratic Lagrangian of the form

$$L$$

A. Island size

The map 21) has rich dynamical behavior which has only been partially explored. One experiment that illustrates some of the phenomena is the computation of the size of the stable island around the elliptic fixed point. For the two-dimensional case this experiment was first performed by Hénon.[30] Those calculations clearly showed the strong dependence of the size of the island on the residue, and in particular that it shrinks to zero at the $5\frac{1}{3}$ resonance. Hénon used the length of the portion of the symmetry line that contains bounded orbits as an estimate for the area of the island. The actual area of the island can also be computed by ''counting pixels'' that contain trapped initial conditions,[32] or by the more efficient and precise method of exit time distributions.[22]

The quadratic map 21) does have reversing symmetry with a fixed set $\{x\,5\,0\}$. Thus, by analogy with Hé

sector the boundary of the island is estimated by considering an orbit as trapped if it does not leave the cube of bounded orbits for 1000 iterations. The transition point on each ray is found by bisection. This is much more efficient than counting pixels would be, particularly for large islands, though it does rely on the assumption of star convexity.

We observe that the island size is strongly influenced by the low order resonances. In the left panel, the area shrinks to zero near and outside the 301) and 031) resonances, while in the right panel the 210) resonance is most effective. Many of the resonances shown in Fig. 6 are visible in particular in the right picture. The fact that the 110) resonance increases the island size instead of decreasing it) is related to the fact that under the strong-stability assumption, our map is diagonalizable when $_1 \neq _2$; generically, this would not be the case, and the 110) resonance might have a strong effect in the opposite way.

For four-dimensional maps an explicit volume calculation by counting ''voxels'' is prohibitively expensive; however, the exit time distribution technique[22] is much more efficient and can still be carried out. To do this, we choose a hypercube $C = \{|x|,|y| < 2\}$ that appears to contain all of the bounded orbits. Moser[29] gives a larger box that contains all bounded orbits, but from our numerical experiments we see that for our parameters C is sufficient. The incoming set for C is the portion of the cube that is not in its image, $I = C \setminus f(C)$. The exit time, $t^{-1}(z)$ for a point $z \in I$, is the number of iterations until it leaves C, and the average exit time, $\langle t^{-1} \rangle_I$, is the average over all points in I. If we compute this average, then the volume of the accessible region is given by $\langle t^{-1} \rangle_I \mu(I)$. Thus the volume of trapped orbits is $\mu(C) - 2\langle t^{-1} \rangle_I \mu(I)$, where μ is the measure of the respective sets.

The exit time computation is realized as a Monte Carlo simulation. First pick a random point in the cube C. If its preimage is in C, then it is not in I, and it is discarded; otherwise, determine the exit time of the point. The average over all such points is $\langle t^{-1} \rangle_I$. The probability P_I of a point to be in I gives $\mu(I) \approx P_I \mu(C)$. In this Monte Carlo realization, statistical fluctuations can give an accessible volume slightly larger than $\mu(C) - 4^{-4}$. In this case the trapped area is set to be 0.

Typical results are shown in Fig. 8, for the same parameters as in Fig. 7. The results are qualitatively similar to the previous one, though the volume drops more dramatically near higher order resonances than the area on the symmetry plane does, presumably because volume has sampled new regions of phase space.

B. Normal form

To transform 21) to Birkhoff normal form it is conve-

For certain terms this will give $m_1 = m_2 = 0$, in which case the corresponding term can never be removed by a coordinate transformation. The coefficients of these irremovable terms are called the twists. In the present case up to degree 3 they are given by z_1, $z_1(z_1\overline{z_1})$, z_1

the numerator of the rational expression for $\det_{\gamma 0}$ from 29) and set it to zero, since this eliminates infinities which are unimportant in drawing the zeros. We show examples of these curves in Fig. 10 for the same parameter values as Fig. 9.

In general the expression for the twistless bifurcation curves in parameter space are quite complicated. However, the poles in $\det_{\gamma 0}$ that occur at low-order resonances are helpful in understanding the behavior, just as they were helpful in the two-dimensional case.[3]

nances, poles of order two at the 210) *and* 120) *resonances and poles of order one at the* 201), 021), 301) *and* 031) *resonances. The coefficients of the second and third order poles are always negative*.

Proof

close to the two neighboring codimension-two points corresponding to vanishing of each column of τ_0, e.g., near $R = (0.35, 0.89)$ in Fig. 11. For example, if we allow a_{30} to vary from our standard choice of equal parameters, we find that the matrix τ_0 vanishes identically when $R \approx (0.348\,41, 0.896\,33)$ and $a_{30} = 1.526\,63 a_{21}$. This corresponds to a simultaneous ''crossing'' of the three curves of zero twist matrix entries; this is not a persistent crossing—it corresponds to the vertex of the cone defined by the vanishing of the determinant of a symmetric matrix.

B. Frequency maps

In this section we will obtain some frequency maps for 21) using Laskar's method.[21] The basic idea is to approximately compute the frequencies for a particular initial condition by iterating for some fixed, finite time 9.97by iterating for somes method18.7342 -1.2 TD [(sponds)-376.1(t1(a)-88muencies)muen

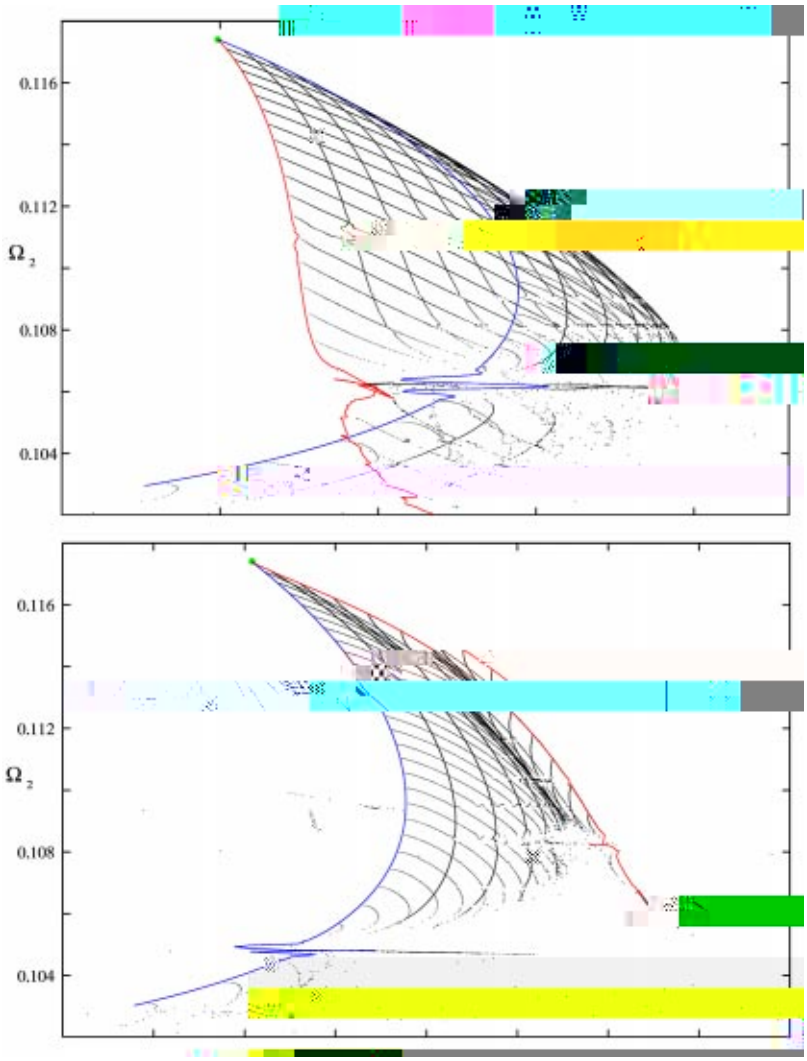

FIG. 13. Col(the)x 13.

a FFT for this because we need very high accuracy in Ω_1. To find the second frequency, Ω_2, we remove the first frequency from the signal by forming $w_t = v_t - 2e^{-2\pi i \Omega_1 t} F(v;\Omega_1)$. Then $F(w;\Omega_2)$ is maximized. Frequencies are only defined up to unimodular transformations. When changing the parameters it is therefore possible that the largest peak appears at a different linear combination. To avoid such discontinuities in the frequency map we use a continuation method that tries to find local maxima near the previously found maxima.

In Fig. 12 parameters are chosen for the two panels on opposite sides of the $\det_{\gamma_0} = 0$ curve. Here the top panel

shows that the twist columns are nearly antiparallel, and in

[3] R. Moeckel, ‘‘Generic bifurcations of the twist coefficient,’’ Ergodic Theor. Dyn. Syst. **10** 1), 185–195 1990).
[4] H. R. Dullin, J. D. Meiss, and D. Sterling, ‘‘Generic twistless bifurcations,’’ Nonlinearity **13**, 203–224 1999).
[5] J. P. van der Weele, T. P. Valkering, H. W. Capel, and T. Post, ‘‘The birth of twin Poincaré–Birkhoff chains near 1:3 resonance,’’ Physica A **153**, 283–294 1988).
[6] J. P. van der Weele and T. P. Valkering, ‘‘The birth process of periodic-orbits in non-twist maps,’’ Physica A **169**, 42–72 1990).
[7] T. P. Valkering and S. A. Vangils, ‘‘Bifurcation of periodic-orbits near a frequency maximum in near-integrable driven oscillators with friction,’’ Z. Angew. Math. Phys. **44** 1), 103–130 1993).
[8] C. Simó, ‘‘Stability of degenerate fixed points of analytic area-preserving mappings, bifurcation, ergodic theory and applications,’’ Astérisque **98**, 184–194 1982).
[9] H. E. Cabral and K. R. Meyer, ‘‘Stability of equilibria and fixed points of conservative systems,’’ Nonlinearity **12**, 1351–1362 1999).
[10] J. E. Howard and S. M. Hohs, ‘‘Stochasticity and reconnection in Hamiltonian systems,’’ Phys. Rev. A **29**, 418–421 1984).
[11] J. E. Howard and J. Humpherys, ‘‘Nonmonotonic twist maps,’’ Physica D **80**, 256–276 1995).
[12] A. D. Morozov, ‘‘Degenerate resonances in Hamiltonian systems with 3/2 degrees-of-freedom,’’ Chaos **12**, 539–548 2002).
[13] C. Simó, ‘‘Invariant curves of analytic perturbed nontwist area-preserving maps,’’ Regular Chaotic Motion **3** 3), 180–195 1998).